united nations
educational, scientific
and cultural
organization

international atomic
energy agency

the
abdus salam
international centre for theoretical physics

SMR.1511 - 7

Third Stig Lundqvist Conference on Advancing Frontiers of Condensed Matter Physics:

"Fundamental Interactions and Excitations in Confined Systems"

11 - 15 August 2003

Theoretical Studies of Nanotubes, Nanocrystals and some Molecular Systems

Marvin L. COHEN
University of California
Department of Physics
366 Le Conte Hall
Berkeley, CA 94720-7300
U.S.A.

ELSEVIER

Materials Science and Engineering C 15 (2001) 1–11

MATERIALS SCIENCE & ENGINEERING C

www.elsevier.com/locate/msec

Nanotubes, Nanoscience, and Nanotechnology

Marvin L. Cohen *

Department of Physics #7300, University of California and Materials Sciences Division, Lawrence Berkeley National Laboratory, Berkeley, CA 94720, USA

Abstract

The theoretical underpinnings of the properties of nanostructures has become a frontier activity in materials science. Although ab initio and empirically based calculations of the properties of bulk materials and their surfaces have advanced significantly in the past several decades, the extension of these methods to nanocrystals, nanotubes, and large molecular structures is not trivial or automatic. However, considerable progress has been made. Here, we review the status of the theoretical efforts to predict and explain properties of bulk solids and then describe extensions and applications to nanoscience and nanotechnology. © 2001 Elsevier Science B.V. All rights reserved.

Keywords: Nanotubes; Nanoscience; Nanotechnology

1. Theoretical background

The development of quantum mechanics in the 1920s and 1930s and its successes in explaining the detailed properties of atoms and many solid-state phenomena suggested that explaining and predicting real material properties would be forthcoming in a relatively short period of time. However, this was not the case. Because atomic spectra are sharp, their quantum interpretation in terms of electronic transitions between narrow energy levels was relatively easy compared to the broad spectra common to most solids. In contrast to gases of weakly interacting atoms, the solid-state "energy levels" are spread into bands, and because of the strong interactions between the atoms making up a solid, there are crystal field and correlation effects influencing the behavior of the electrons, which in turn have a major effect on many of the properties of solids. Hence, the developments in this field came slowly. Physical models changed as more was learned about the relative importance of the various interactions, and computational techniques were refined so that the resulting equations describing the electronic and lattice properties could be solved. In fact, the major advances in interpreting solid-state band spectra appeared in the 1960s [1].

The evolution continued, and now there is a "Standard Model of Solids" [2], which can be viewed as a set of cores containing periodically arranged nuclei with their core electrons and a sea of valence electrons which interact with the positive cores and with each other (Fig. 1). Some versions of this model account for the detailed electronic structure of the core electrons, but here we ignore the core structure and focus on the approach where the core interaction is treated using a pseudopotential. Hence, the model involves accounting for core–core Coulomb interactions, electron–core interactions computed via pseudopotentials, and electron–electron interactions, which can be evaluated using density functional theory. The approach [2] is robust and allows calculations of electronic structure, crystal structure, lattice vibrations, elastic constants, superconductivity, properties, etc.

The development of the pseudopotential was central to the implementation of the theory. The important concept was the creation of a potential which described the interactions between the valence electrons and the cores. A useful empirical approach to account for these interactions and the electron–electron interactions was developed in the 1960s and is still being used. It is the Empirical Pseudopotential Method (EPM) in which a few parameters are fit to optical data [1]. This approach produced excellent band structures, especially for semiconductors. It also yielded optical spectra and electronic charge density maps. The method was based on the idea [3] that valence electrons experience both an attractive Coulomb core potential and a repulsive Pauli potential arising from the fact that the valence electron wavefunctions must be orthogonal to the core electron wavefunctions. The cancellation of the attractive and repulsive terms leaves a net weak pseudopotential.

* Tel.: +1-510-642-4753; fax: +1-510-643-9473.
E-mail address: mlcohen@uclink.berkeley.edu (M.L. Cohen).

PII: S0928-4931(01)00221-1

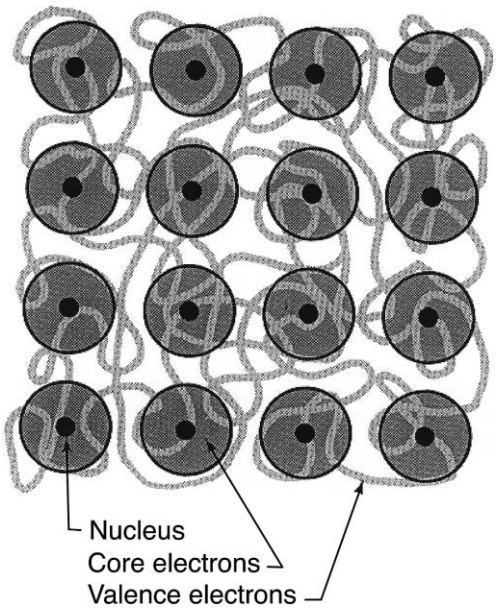

Fig. 1. Model of a solid with cores at fixed lattice positions and valence electrons free to move throughout the crystalline solid.

Hence, the EPM approach involves fitting just the first few form factors to optical data.

The transition from using the EPM approach to an ab initio approach went through several stages. The availability of electronic charge density maps [4] allowed the separation of the total potential into an electron–core potential describable by a pseudopotential and an electron–electron potential which contained the usual Hartree and exchange-correlation contributions. Using a Poisson equation and approximations by Slater [5] and Wigner [6], this method could be applied. The major motivation for this stage of evolution of the method was to use it to compute properties of surfaces and interfaces. Because of charge rearrangement at a surface, it is critical to compute the electronic structure self-consistently and account for the changes in the charge density arising from the structural changes. Hence, electron–electron potentials based on the total charge density $\rho(\vec{r})$ allowed the development of realistic potentials which when added to the electron–core pseudopotentials could reproduce the effects of surface charge rearrangements. However, there still remained the problem of computing the electronic structure since the previous techniques were based on having a bulk crystal with an infinite array of unit cells.

To account for surface and interface geometries and still retain the fundamental approach used to calculate properties of bulk crystals, the concept of a supercell was introduced [7]. The supercell was constructed to contain a slab of atoms with a vacuum region so that infinitely repeated supercells would resemble a system with an infinite number of slabs separated by vacuum. The surfaces of the slabs were good models for crystal surfaces [8], and interfaces could be modeled with two slabs in contact representing different materials [9] to represent systems such as Schottky barriers or heterojunctions.

The supercell concept [7] could be applied to other localized configurations in addition to surfaces and interfaces. An early application was its use in describing the properties of molecules. Here, some geometric arrangement of atoms is repeated in a supercell, which contains enough in the way of vacuum region to prevent molecule–molecule interaction. The result is a model for an infinite array of non-interacting molecules, and hence the computed electronic and structural properties are appropriate for a single molecule. The obvious extension to nanostructures is to build a supercell with a good representation for a nanocrystal, nanotube, large molecule, or whatever nanosystem is of interest and then use the techniques developed for bulk materials to solve for the physical properties of these systems. This is a desirable path; however, the computer time needed to solve the appropriate equations rises quickly with the number of atoms in the unit cell. One then has two choices: (1) reduce the complexity of the cell, mainly by reducing the number of atoms used to model the nanostructure, or (2) use a less sophisticated method for computing the electronic structure so that solving the equations requires less time. Examples of the latter include using the EPM or tight-binding approaches instead of full self-consistent pseudopotential methods. Both of these approximations have been used with success.

The pseudopotential approaches introduced so far, based either on experiment or on analytic expressions used to reproduce the electron–core and electron–electron potentials, evolved into an ab initio or first-principles approach. In this approach, the only input was the atomic number to produce a pseudopotential to account for the core–valence electron interaction. The electron–electron interactions were determined using a density functional approach. Both of these developments had their roots in the 1930s with Fermi's [10] introduction of an atomic pseudopotential and Dirac's [11] development of density functional theory (DFT). More modern versions of pseudopotentials [12–17] and DFT [18,19] are part of the Standard Model, and there is constant evolution in this very active area of condensed matter physics.

Using the above scheme in principle constitutes the Standard Model referred to earlier. In practice, the pseudopotentials are usually generated to reproduce the outer portions of the electronic wavefunctions but not the region near the core which can have fairly complex oscillatory behavior. The local density approximation (LDA) to DFT is often used to calculate ground-state properties and excited state spectra are often evaluated using a "GW" approximation [20]. One of the first applications [21] was to the structural properties of Si. A momentum-space formalism [22] was used to compute total energies for different structural forms of Si. By comparing the resulting total energies, the lowest energy structure for each volume

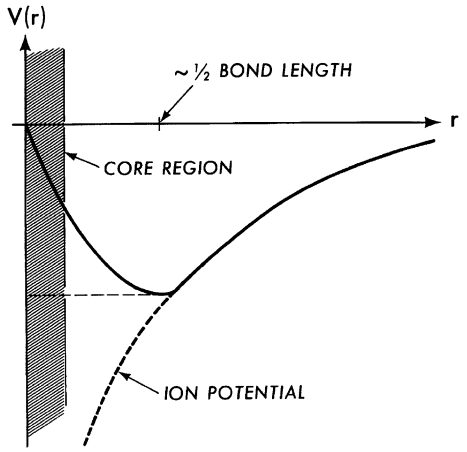

Fig. 2. Schematic plot of a pseudopotential as a function of position compared with an ionic Coulomb potential.

could be determined, and this allowed a determination of the high pressure phase structures and many ground-state properties.

Examples of applications of the theories described above are given in Section 2.

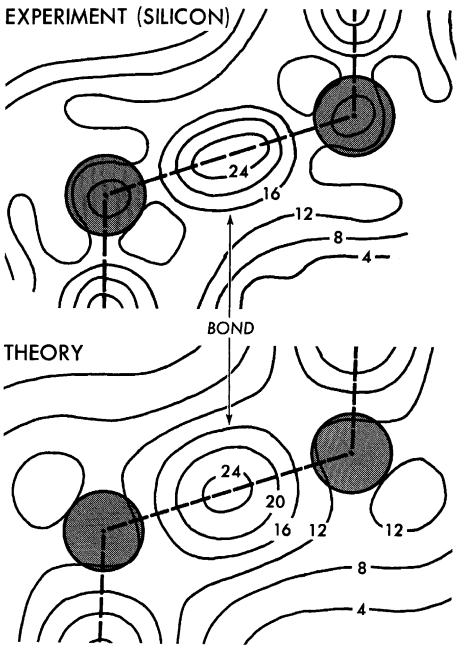

Fig. 4. The valence electron charge density of silicon. Contour spacings are in units of electrons per unit cell volume. Shaded circles represent atomic cores.

2. Applications to bulk materials

The EPM described above used data to fit Fourier form factors $V(\vec{G})$ of the pseudopotential $V(\vec{r})$. When $V(\vec{r})$ is weak, only the first few $V(\vec{G})$s are needed, which is,

$$V(\vec{r}) = \sum_{\vec{G}} S(\vec{G}) V(G) e^{i\vec{G}\cdot\vec{r}} \quad (1)$$

where $\vec{G}$ is a reciprocal lattice vector and $S(\vec{G})$ is the structure vector which is used to locate the atoms in the primitive cell. In practice, three $V(G)$s per atom are sufficient. A schematic picture of the resulting potential is shown in Fig. 2 along with an ion (or Coulomb) potential for comparison. The form factors are generally overdetermined when the computed optical spectrum is compared with measured reflectivity or modulated reflectivity data [1]. Features in the optical spectrum can be associated with critical points in the electronic band structure $E_n(\vec{k})$, where n is the band index and $\vec{k}$ is the crystal wavevector. In particular, for a direct optical transition between bands i and j, when

$$\nabla_{\vec{k}} E_i(\vec{k}) = \nabla_{\vec{k}} E_j(\vec{k}), \quad (2)$$

a critical point at that value of $\vec{k}$ occurs, and there is a resulting Van Hove singularity in the optical spectrum. These singularities are particularly evident in modulated spectroscopy as shown in Fig. 3.

By analyzing optical spectra in the manner described above, it was possible to obtain the electronic band struc-

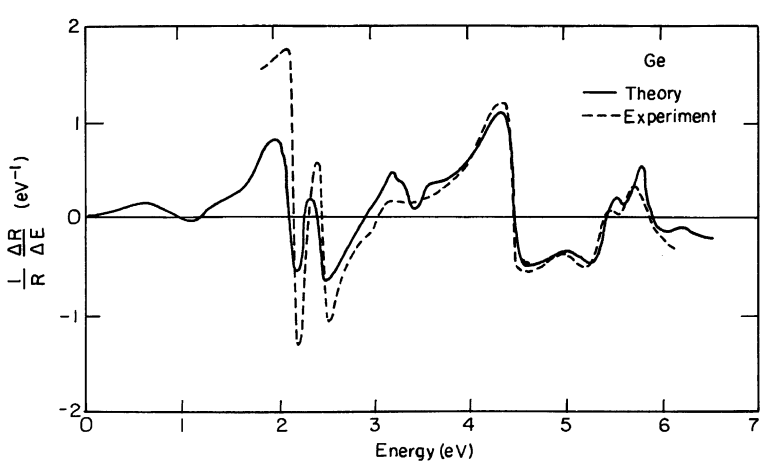

Fig. 3. Measured and calculated derivative reflectivity spectra for germanium.

ture and wavefunctions. From these, the optical constants, densities of states, photoemission spectra, and electron charge density maps can be obtained. An example of the latter is shown in Fig. 4 where the predicted electronic charge density is compared with experiment.

Hence, in principle, the problem of electronic structure outlined before as a goal of quantum theory was solved. The approach worked well for bulk semiconductors, insulators, and metals. In addition, using the supercell approach described above, this method was applied to surfaces, interfaces, and small molecules after analytic forms were used for the potentials.

As described in the Section 1, the extension to the current ab initio approach required first-principles pseudopotentials, density functional theory, and a reliable method to calculate total energies. An example of the application of this approach to ground-state properties is its use in determining the structural, electronic, and vibrational properties of Si. By evaluating the total energy for a given volume, it is possible to determine the lowest energy structures as a function of volume. The caveat is that only a finite, and often small, number of candidate structures are considered. For the Si example, seven structures (diamond, hexagonal diamond, β-tin, sc, fcc, bcc, and hcp) are shown in Fig. 5. Other structures are known for Si, such as the BC8 structure, which is found experimentally under certain conditions. Although it is straightforward to calculate the properties of BC8 Si, at this point, it is not easy to guess beforehand that this structure would be a good candidate for a low energy structure. Hence, we are not yet at the point where ab initio theory is capable of predicting structures in general; however, it is possible to compare candidate structures. Progress in molecular dynamics [23], used in conjunction with the methods described here, suggests that this goal may be achieved, or, at the least, theory will be more fruitful in predicting new structures in the future.

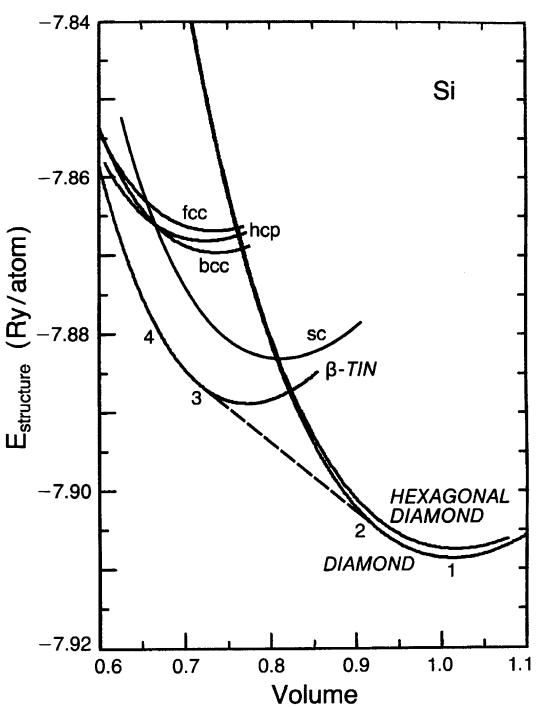

Fig. 5. Total energy curves for seven structures of Si as a function of volume normalized to the experimental volume. The dashed line is the common tangent between the diamond and the β-tin phase.

Returning to the Si example, the structural energy has several parts, including: kinetic energy of the electrons and cores; core–core Coulomb interactions; electron–core terms; and electron–electron Coulomb, exchange, and correlation effects. Using pseudopotentials, the total energy formalism, and the LDA, these can all be evaluated [2] and the total or structural energy $E_{\text{structure}}$ can be evaluated as a function of volume. The results in Fig. 5 show that diamond is the lowest energy structure and the resulting volume and energy dependence on volume at this energy yields a lattice constant and bulk modulus in excellent agreement with experiment. Typical expected precision for this method is less than 1% for lattice constants and around 5% for bulk moduli and other elastic constants. These results are impressive when one considers the limited input of the atomic number and crystal structure.

As pressure is increased, there is the subsequent volume decrease and, as shown in Fig. 5, other structural phases have lower energy than the diamond structure. Hence, this approach is capable of computing transition volumes and the transition pressure for a structural phase change. This is illustrated in Fig. 5 by the common tangent drawn between the diamond and β-tin phases. At volumes corresponding to points 1 and 4, the diamond and β-tin structural phases are found, respectively. However, for the region between points 2 and 3, the transition is occurring. The slope of the common tangent yields the transition pressure and the volumes at points 2 and 3 are the transition volumes. Excellent agreement between theory and experiment is obtained for these quantities.

Besides ground-state structural properties, the total energy pseudopotential method can be used to determine phonon dispersion curves and electron–phonon interactions [2]. A particularly impressive result is the calculation for simple or primitive hexagonal (sh or ph) and hcp Si. For these structural phases, not only the electronic and ground-state structural properties were determined from first principles, a calculation of the electron–phonon couplings led to a successful prediction of superconductivity in these metallic phases and excellent estimates of the superconducting transition temperatures.

3. Nanocrystals

The physics, chemistry, and engineering of nanocrystals has evolved considerably in recent years, and this area has

become a challenge for theory. In our previous discussion on bulk crystals, their periodic nature was fixed which resulted in simplifying and useful concepts such as Bloch wavefunctions to exploit translational invariance. We also described the complications introduced by surfaces and interfaces, which break the translational invariance and introduce the possibility of electronic charge rearrangement and atomic reconstruction. One method for dealing with these changes is to restore periodicity through the use of a supercell [7]. Similar techniques can be used for nanocrystals, but the resulting computer calculations become formidable. Two other techniques and applications will be described here.

The goal of theory is to explain size and shape effects in these systems where many of the constituent atoms are near the surface of the nanocrystal. Hence, there are the effects of confinement and shape to explore, and the cases discussed here will be semiconductor nanocrystals containing hundreds to thousands of atoms. The two theoretical approaches presented are the Wannier function approach and the Green function approach. For the Wannier function method, some applications will be given, whereas only the formalism of the Green function method will be described as applications have not yet been reported.

Wannier functions are localized wavefunctions, which can be expressed in terms of Bloch wavefunctions [24]:

$$a_n(\vec{r}-\vec{R}) = \frac{1}{\sqrt{\Omega}} \int_{\mathrm{BZ}} \mathrm{d}^3k \mathrm{e}^{-i\vec{k}\cdot\vec{R}} \Psi_{n,\vec{k}}(\vec{r}) \tag{3}$$

where $a_n(\vec{r}-\vec{R})$ and $\Psi_{n,\vec{k}}(\vec{r})$ are Wannier and Bloch functions, respectively, $\vec{R}$ is a lattice vector, and Ω is the volume of the Brillouin zone (BZ). The Wannier functions are localized around lattice sites, and they are used as basis sets for tight-binding calculations where the energy:

$$E_n(\vec{R}) = \frac{1}{\Omega} \int_{\mathrm{BZ}} \mathrm{d}^3k \mathrm{e}^{-i\vec{k}\cdot\vec{R}} E_n(\vec{k}) \tag{4}$$

A calculation for a bulk crystal involves taking matrix elements of the bulk Hamiltonian H_{B} between Wannier functions to obtain $E_n(\vec{R})$ in a tight binding like scheme. For a nanocrystal, one can consider the Hamiltonian to be:

$$H_{\mathrm{N}} = H_{\mathrm{B}} + (U_{\mathrm{N}} - U_{\mathrm{B}}) \tag{5}$$

where the difference in potentials between the nanocrystal and the bulk crystal is expected to be reasonably approximated by:

$$U_{\mathrm{N}}(\vec{r}) - U_{\mathrm{B}}(\vec{r}) \approx \begin{cases} 0 & \vec{r} \quad \text{inside} \\ \infty & \vec{r} \quad \text{outside} \end{cases} \tag{6}$$

to account approximately for the boundary conditions on the nanocrystal. The result [25] is that approximate eigenstates and eigenvalues of H_{N} can be obtained by diagonalizing:

$$\left\langle a_{n,\vec{R}_i} \middle| H_{\mathrm{N}} \middle| a_{m,\vec{R}_j} \right\rangle \approx \delta_{m,n} E_n\left(\vec{R}_i - \vec{R}_j\right) \tag{7}$$

One application which illustrates the improvement of the Wannier function approach over a simpler effective mass approximation is the study of InAs nanocrystals [26]. The approach starts with an EPM calculation of the bulk band structure which yields Bloch functions and, via Eq. (3), the Wannier functions. The Wannier states are used to diagonalize the Hamiltonian and the electronic structure can then be computed as a function of the nanocrystal radius. The result for the fundamental gap of InAs appears in Fig. 6 along with experimental photoluminescence data [27]. A calculation based on $\vec{k}\cdot\vec{p}$ theory [28] is also shown in Fig. 6 for comparison. In contrast to the $\vec{k}\cdot\vec{p}$ approach, the Wannier function results are in excellent agreement with experiment. The failure of the "effective mass" approximations such as the one used in the $\vec{k}\cdot\vec{p}$ approach is most likely attributable to the assumption of a parabolic, spherical band dispersion over a large part of the BZ. For smaller nanocrystals, one expects that their properties will be greatly influenced by band structure states at large $\vec{k}$ where the assumption of parabolic bands breaks down.

Another interesting application of the Wannier function approach to nanocrystals is the study of the pressure dependence of band states in InP. For the bulk crystal, the gaps between the top of the valence band and the bottom of the conduction band behave differently as a function of $\vec{k}$. Measured from the valence band maximum, the conduction band minimum at Γ moves up in energy with increasing pressure more rapidly than the L minima which also move up. In contrast, the minima at X move down with increasing pressure. Hence, the direct (Γ–Γ) gap at ambient pressure will no longer be the minimum gap at high pressure. As the state at X lowers, an indirect gap (Γ to X) becomes the fundamental gap. This pressure-induced direct to indirect gap transition in the bulk can have different

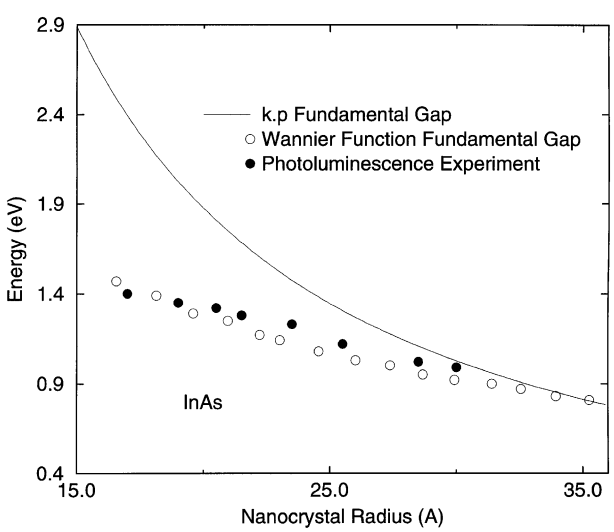

Fig. 6. Lowest energy gap of InAs nanocrystal versus radius.

characteristics in an InP nanocrystal. In particular, the quantum confinement of the conduction band states can influence the pressure dependent properties of the energy bands. One can argue that because of confinement, the localization in real space will result in a "delocalization" in *k*-space leading to conduction band states, which are averaged over the BZ. Hence, a characteristic conduction state could have Γ, X, and L mixing.

The calculational results [29] for the InP nanocrystal energy levels indicate that confinement energies are relatively insensitive to pressure. Because the confinement reduces the Γ–X separation, these studies suggest that it would require less pressure to induce an indirect transition in InP nanocrystals than in the bulk semiconductor. The model chosen here is for a nanocrystal with an equal number of In and P atoms. Different ratios of the atoms may have an effect on these conclusions. The dependence of the bulk and nanocrystal energy levels on the relative change in lattice constant $\Delta a/a$ is shown in Fig. 7.

The applications of the Wannier function method to InAs and InP given above are examples of the "state of the art" in calculating properties of semiconductor nanocrystals. The Wannier method can be applied broadly and it is computationally tractable for many applications. Another theoretical approach using Green functions which has conceptual appeal is suggested next, but it has not yet been used broadly for computation of material properties.

The motivation for the Green function approach is to attempt to use bulk descriptions via Green functions and modify these for nanocrystals. For many studies, the electronic wavefunctions of the systems investigated are not needed, but determining the energy spectrum is the objective. In this case, having the Green function to use in obtaining quantities such as the density of states is very useful. The goal is to develop a formalism in which the confined Green function $G_c(\vec{r},\vec{r}',E)$ is expressed in terms of the bulk Green function $G_b(\vec{r},\vec{r}',E)$ as:

$$G_c(\vec{r},\vec{r}',E) = G_b(\vec{r},\vec{r}',E) + \Delta G(\vec{r},\vec{r}',E) \quad (8)$$

where $\Delta G(\vec{r},\vec{r}',E)$ is the perturbation arising from the differences between bulk and nanocrystal environments.

The form of Eq. (8) is consistent with what one expects intuitively since a nanocrystal is often viewed as a small part of a bulk crystal with perturbations arising from confinement, shape, and surface effects. The results above for InAs pressure coefficients of band states is suggestive of this view. To a first approximation, the nanocrystal and bulk coefficients are similar. The difficulty is to treat the boundary conditions for the nanocrystal in an appropriate way. A theoretical basis for Eq. (8) has been developed [30] and some tests have been made. One of the advantages of the Green function method is that it deals directly with spectral functions. Hence, as an example, in principle, one could expect to be able to calculate optical properties using response functions appropriate for the bulk crystal plus a " nanocrystal perturbation". The expression of the frequency dependent imaginary part of the dielectric function is

$$\varepsilon_c^{(2)}(\omega) = \varepsilon_b^{(2)}(\omega) + \Delta\varepsilon^{(2)}(\omega) \quad (9)$$

A calculation based on perturbing the bulk spectral properties to obtain nanocrystal properties would be highly desirable.

Hence, there are theoretical techniques for dealing with the unusual effects which arise from geometry and confinement. Some examples are those discussed here: the supercell method and the Wannier and Green function approaches. This general area of theory is still evolving both conceptually and from the point of view of applications.

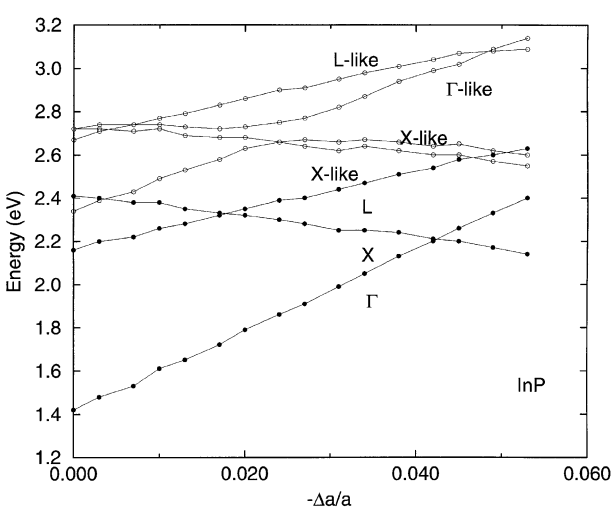

Fig. 7. Unoccupied states (unfilled circles) of InP 27 Å diameter nanocrystal versus reduced lattice constant induced by pressure. Bulk states are filled circles.

4. Nanotubes

A motivation in nanoscience is to try to understand how materials behave when sample sizes are close to atomic dimensions. There is also the opportunity to use nanostructures for technology. One goal of device science is miniaturization, hence nanotechnology has received considerable attention. There is also the possibility that the unique properties of nanostructures will result in novel applications and devices. Another reason for the great popularity of this field is that phenomena occurring on this length scale are of interest to physicists, chemists, biologists, electrical and mechanical engineers, and computer scientists. Although many nanostructures such as large molecules and quantum dots are of interest, at present, one of the most active areas is the study of nanotubes.

Carbon nanotubes were discovered [31] in 1991. They are found as single-walled tubes, multi-walled tubes (con-

centric tubes), and they sometimes bunch to form "ropes". Other nanotubes exist, such as those based on Mo [32], and some (BN, BC_2N, BC_3, and CN) have been predicted [33–36] using the theoretical methods described earlier.

For all of the $B_xC_yN_z$ tubes, sp^2 bonding plays a fundamental role. The classic example of the difference between sp^3 and sp^2 bonding properties is how carbon forms diamond and graphite. For diamond, the three-dimensional, four-fold coordinated sp^3 structure is rigid and almost isotropic in its properties. In contrast, the graphite sp^2 bonding is planar and three-fold coordinated in the planes with weak bonding between the planes. The strong covalent in-plane bonding and weak van der Waals interplane bonding results in anisotropic physical properties which are useful for applications to lubrication and other processes requiring "slippage" between layers. The in-plane carbon–carbon bonds are shorter than those of diamond, but the interlayer distances are large. The nature of the bonding is shown in Fig. 8.

One can view a single-walled carbon tube as a rolled up sheet or strip of sp^2-bonded graphene. The atoms are located using a pair of integers (n,m) and the lattice vector $\vec{C} = n\vec{a}_1 + m\vec{a}_2$ as shown in Fig. 9. A tube can be classified using the pair of integers by viewing the rolling up of the sheet as the "placement" of the atom at (0,0) on the atom at (n,m). Hence, different diameter tubes and helical arrangements of hexagons can arise by changing (n,m) as shown in Figs. 10 and 11.

The electronic properties are sensitive to the stricture of the tube. Carbon nanotubes can be metallic or semiconducting depending on (n,m). For example, if $n-m$ is three times an integer, the carbon nanotube has an extremely small gap, and at room temperature, it has metallic behavior. For $n=m$, the tubes are metallic; and for other values of $n-m$, the tubes behave as semiconductors with a band gap. The theoretical explanation [37–39] is based on band folding, starting with the electronic structure of a

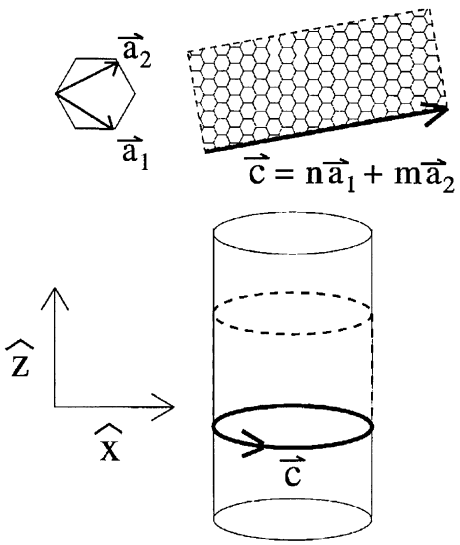

Fig. 9. Structure of an (n,m) carbon nanotube. The carbon atoms are at the vertices of the hexagons.

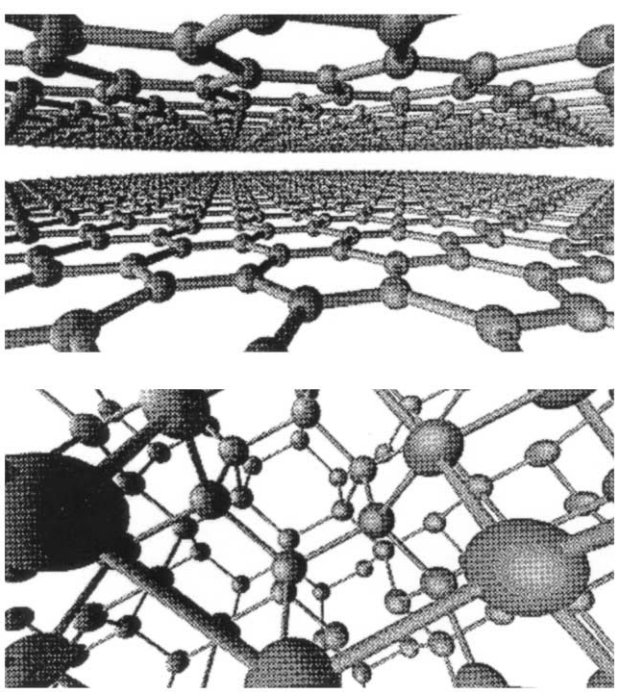

Fig. 8. Contrasting sp^2 bonding (upper) with sp^3 bonding (lower) using ball and stick models.

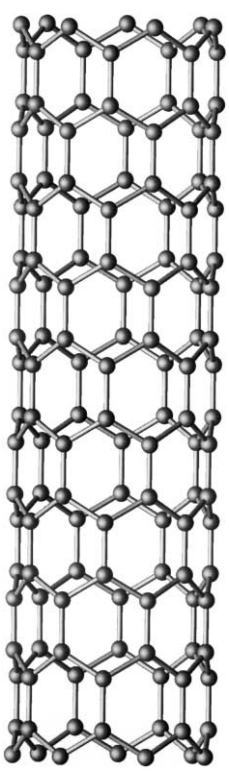

Fig. 10. Ball and stick model for a nanotube. The balls represent carbon atoms.

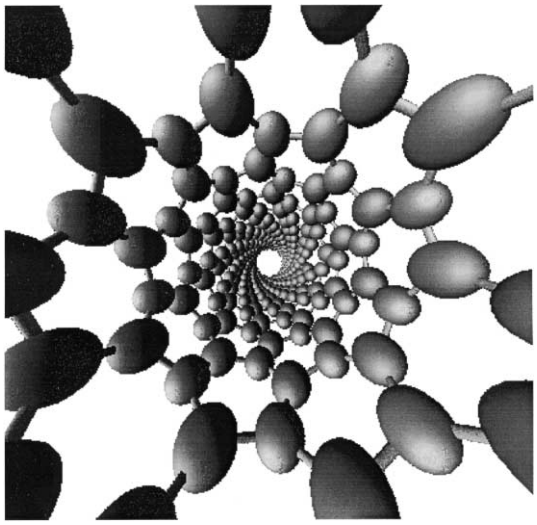

Fig. 11. Schematic structural model of a helical nanotube.

graphene sheet. Some of these predictions have been verified using scanning tunneling microscopy [40,41] (Fig. 12).

Because of their geometry, nanotubes are sensitive to defects and impurities. This sensitivity gives rise to unusual properties. For example, in three dimensions, we are accustomed to the fact that if one metal carrying current is put in contact with a second metal—consider copper and aluminum as an example—then the electrical current will flow across the junction from the first metal to the second. For two metallic carbon nanotubes, depending on the helicity, the junction can stop the current because of the mismatch of wavefunction symmetry [42]. Theoretical studies suggest that breaking the symmetry by bending the tubes will allow the flow of current.

Another example which may lead to a useful device is the junction between a semiconductor and a metallic carbon nanotube. In Fig. 13, two tubes are shown joined by a

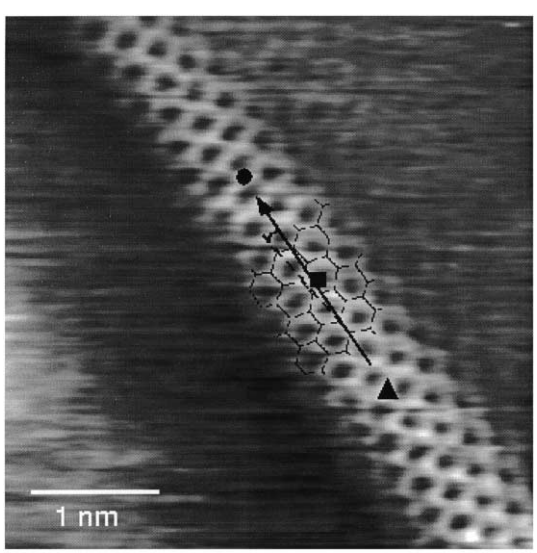

Fig. 12. Low temperature STM images of a carbon nanotube [41].

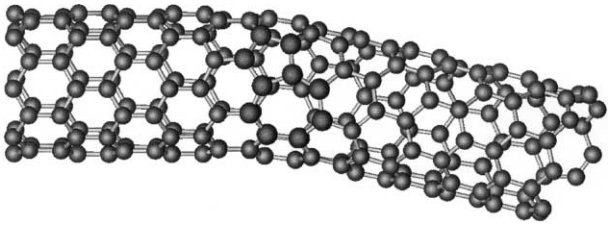

Fig. 13. A carbon nanotube Schottky barrier formed from an (8,0) semiconductor nanotube joined by a 5–7 defect to a (7,1) metallic nanotube.

defect [43]. The defect involves the rotation of bonds between two hexagons to form a five-fold ring and an adjacent seven-fold ring. This defect allows the joining of a semiconducting (8,0) tube with a semi-metallic (7,1) tube and the junction is in effect a Schottky barrier or quasi-1D semiconductor/metal junction made from a single element (Fig. 14). Calculations of the local densities of states for this system yield spectra which are very similar to those evaluated for 3D systems. Far from the interface on the (8,0) side of the device, there is an energy gap, while on the (7,1) side, there are states at the Fermi level. Near the junction, metal-induced gap states similar to those found for standard 3D Schottky barriers are found.

One can extend the above arguments to consider two semiconductor nanotubes used for a heterojunction. One such system would be an (8,0) tube in contact with a (5,3) tube. Again, defects can be arranged so that these two tubes will join and local densities of states are obtained which are similar to those obtained for standard 3D semiconductor/semiconductor junctions.

The examples above focus on pure carbon nanotubes, however, compound $B_xC_yN_z$ nanotubes offer another variable, i.e. chemical composition changes in addition to

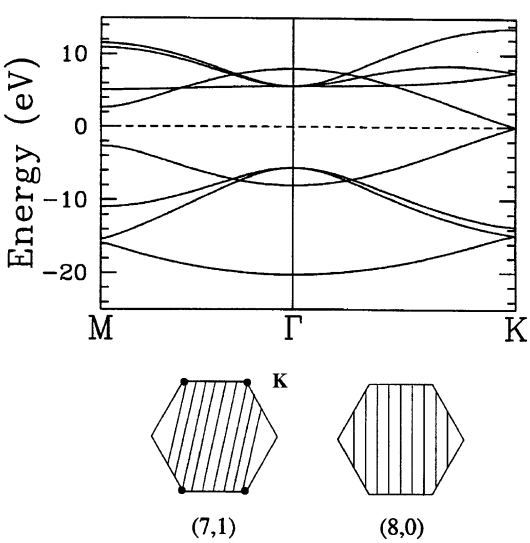

Fig. 14. Electronic band structure of graphene, which is a single sheet of graphite (upper). Brillouin zones for graphite with allowed $\vec{k}$ for the (7,1) and (8,0) nanotubes (lower).

geometric and defect-related manipulations of electronic structure. Another example, is the insertion of other elements into nanotubes such as K atoms in a C nanotube [44]. In this example, the outer electron is expected to leave the K atoms, which can form a chain inside the nanotube. The expected effect is that a cylinder of charge will result with electrons coating the inside of the C tube.

A similar electronic effect is expected for a doped BN nanotube. The calculated charge density for states associated with the lowest conduction band is a free-electron-like state which concentrates charge along the center of the tube. Although the prediction [33] of the existence of BN nanotubes has been verified [45], transport properties have not been explored yet. This is similar for BC_2N (Fig. 15), which has a helical structure and is expected to have a chiral arrangement of charge density when doped. Hence, this system is expected to behave like a nanocoil [46]. Another theoretical prediction is that BC_3 tubes will act individually as semiconductors, but bundles of these tubes are expected to exhibit metallic behavior [35].

The experimental activity in the nanotube field is currently very large and broad. Structural properties are studied using electron microscopy. Studies using atomic force microscopy and scanning tunneling microscopy have yielded considerable structural and electronic information. Many of these studies are searching for special effects resulting from the reduced dimensionality and device applications. A few examples include observations of metallic transport and nonlinear on-tube devices including rectifiers [47] and transistors [48], single electron transport [49] (Fig. 16), and behavior suggesting 1D electronic structure

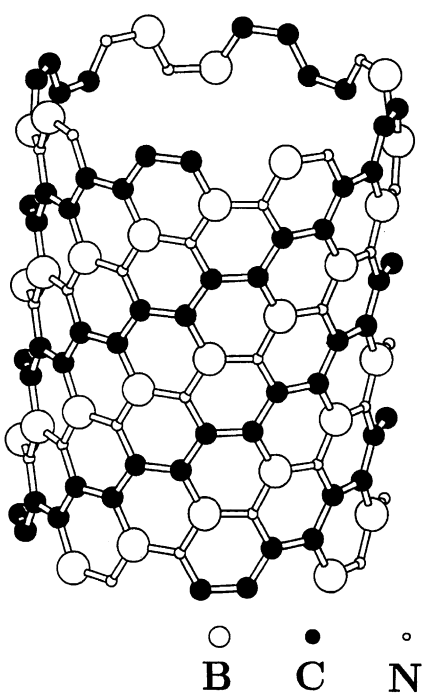

Fig. 15. Ball and stick model of a representative structure of a BC_2N nanotube.

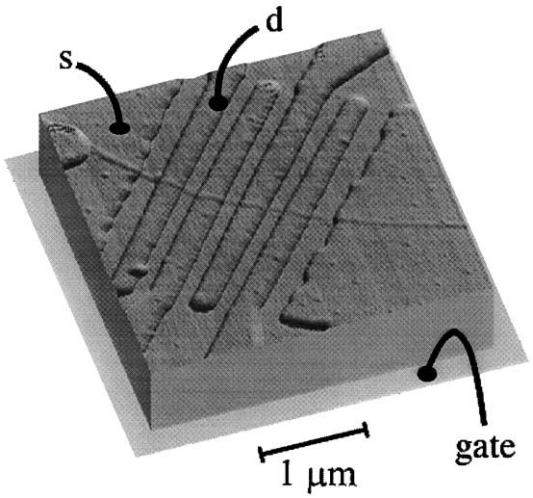

Fig. 16. The arrangement for obtaining transport measurements of a single-walled nanotube rope in reference [49].

[50]. Coulomb blockade characteristics are observed in magnetic field studies of spin–splitting and even–odd effects in a single-walled carbon nanotube rope [51].

Other applications include the possibilities associated with the strength of nanotubes. There have been measurements of the structural stability and elastic constants of C and BN nanotubes [52,53]. These systems have extremely large Young's moduli and it is expected that they will be useful in strengthening existing materials. Other possible applications include electron emitters for flat panel displays [54], lubricants [55], and random access computers [56]. These are just a few of the many possible applications of nanotubes.

The discovery of nanotubes and the associated growth in research on tubes has been associated with the previous discovery of C_{60} [57]. These fullerene systems are of great interest and many studies have been done related to this molecule, solids formed from C_{60}, and A_3C_{60} where A is an alkali metal. Other variations of configurations of C either molecular or planar [58] have been considered just as other compounds have been suggested as possible tube forming systems [59]. In the discussion below, we consider C_{36} [60,61], which has been the subject of recent studies. This example is included to illustrate how variations on the

Table 1
"Standard Model" (pseudopotentials and density functional theory)
The Standard Model describes the following ground-state and excited properties for a broad class of solids, clusters, and molecules.

Electronic structure
Crystal structure and structural transitions
Structural and mechanical properties
Vibrational properties
Electron–lattice interactions
Superconductivity
Optical properties
Photoemission properties

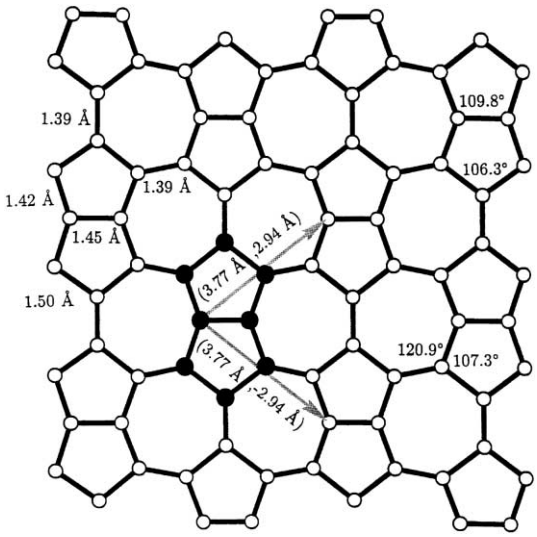

Fig. 17. Structure of carbon pentaheptite formed from five-fold and seven-fold rings of bonds.

structural and electronic properties of the systems described here may lead to more interesting and perhaps useful materials.

Superconductivity in C_{60}-based systems was reported [62] and subsequent studies resulted in relatively high superconducting transition temperatures T_c. Theoretical studies have led to a generally accepted model of BCS electron–phonon induced electron pairing to explain the superconducting properties [63]. Arguments based on the theoretical model suggest that in going from graphite which has a low T_c to the higher T_cs for the C_{60}-based systems, it is the curvature of the hexagonally arranged sheets that is central. This suggests that systems such as C_{36} which has an even higher "curvature" than C_{60} may exhibit superconductivity with a higher T_c. Based on this argument, nanotubes are expected [64] to have moderate T_cs.

A calculation [65] using electron–electron pairing resulting from phonon excitations on the molecule (intramolecular) can be relatively strong for C_{36}-based solids. Estimates of T_c give values in the range of five times that of K_3C_{60}. Hence, these calculations suggest that doped C_{36}-based solids may be superconducting above liquid nitrogen temperatures.

5. Conclusions

The most general conclusion is that new materials often lead to new phenomena and applications, and that on the theory side, the Standard Model appears to be capable of explaining and predicting a large variety of physical properties such as those shown in Table 1.

The variety of structures just using C is extremely broad when one considers the new forms beyond diamond and graphite which have emerged recently: macromolecules such as C_{60}, C_{70}, and C_{36}, onions (concentric buckyballs), single-walled and multi-walled tubes, tori, and variously shaped fragments. In Fig. 17, an example of possible layer-based systems is shown [58]. Systems such as these and variations using B, C, and N should provide interesting building blocks and phenomena for nanoscience and nanotechnology.

Acknowledgements

This work was supported by National Science Foundation Grant No. DMR-9520554 and by the Director, Office of Energy Research, Office of Basic Energy Science, Materials Sciences Division of the U.S. Department of Energy under Contract No. DE-AC03-76SF00098.

References

[1] M.L. Cohen, J.R. Chelikowsky, Electronic Structure and Optical Properties of Semiconductors. Springer-Verlag, Berlin, 1988.
[2] M.L. Cohen, Phys. Scr., T 1 (1982) 5.
[3] J.C. Phillips, L. Kleinman, Phys. Rev. 116 (1959) 287.
[4] J.P. Walter, M.L. Cohen, Phys. Rev. Lett. 26 (1971) 17.
[5] J.C. Slater, Phys. Rev. 81 (1951) 385.
[6] E. Wigner, Phys. Rev. 46 (1934) 1002.
[7] M.L. Cohen, M. Schlüter, J.R. Chelikowsky, S.G. Louie, Phys. Rev. B 12 (1975) 5575.
[8] M. Schlüter, J.R. Chelikowsky, S.G. Louie, M.L. Cohen, Phys. Rev. B 12 (1975) 4200.
[9] M.L. Cohen, in: L. Marton, C. Marton (Eds.), Advances in Electronics and Electron Physics, vol. 51, Academic Press, New York, 1980.
[10] E. Fermi, Nuovo Cimento 11 (1934) 157.
[11] P.A.M. Dirac, Proc. Cambridge Philos. Soc. 26 (1930) 376.
[12] A. Zunger, M.L. Cohen, Phys. Rev. B 18 (1978) 5449.
[13] T. Starkloff, J.D. Joannopoulos, Phys. Rev. B 19 (1979) 1077.
[14] D.R. Hamann, M. Schlüter, C. Chiang, Phys. Rev. Lett. 43 (1979) 1494.
[15] G.P. Kerker, J. Phys. C 13 (1980) L189.
[16] N. Troullier, J.L. Martins, Phys. Rev. B 43 (1991) 1993.
[17] L. Kleinman, D.M. Bylander, Phys. Rev. Lett. 48 (1982) 1425.
[18] P. Hohenberg, W. Kohn, Phys. Rev. 136 (1964) B864.
[19] W. Kohn, L.J. Sham, Phys. Rev. A 140 (1965) 1133.
[20] M. Hybertsen, S.G. Louie, Phys. Rev. Lett. 55 (1985) 1418.
[21] M.T. Yin, M.L. Cohen, Phys. Rev. Lett. 45 (1980) 1004.
[22] J. Ihm, A. Zunger, M.L. Cohen, J. Phys. C 12 (1979) 4409; J. Phys. C 13 (1980) 3095.
[23] R. Car, M. Parrinello, Phys. Rev. Lett. 55 (1985) 2471.
[24] E.I. Blount, in: F. Seitz, D. Turnbull (Eds.), Solid State Physics, vol. 13, Academic Press, New York, 1962.
[25] A. Mizel, M.L. Cohen, Phys. Rev. B 56 (1997) 6737.
[26] A. Mizel, M.L. Cohen, Solid State Commun. 104 (1997) 401.
[27] A.A. Guzelian, U. Banin, A.V. Kadavanich, X. Peng, A.P. Alivisatos, Appl. Phys. Lett. 69 (1996) 1432.
[28] A.I. Ekimov, F. Hache, M.C. Schanne-Klein, D. Ricard, C. Flytzanis, I.A. Kurdryavtsev, T.V. Yazeva, A.V. Rodina, A.L. Efros, J. Opt. Soc. Am. B 10 (1993) 100.
[29] A. Mizel, M.L. Cohen, Solid State Commun. 113 (1999) 189.
[30] A. Mizel, M.L. Cohen, Phys. Rev. B 57 (1998) 9515.
[31] S. Iijima, Nature 354 (1991) 56.

[32] R. Tenne, L. Margulis, M. Genut, G. Hodes, Nature 360 (1992) 444.
[33] A. Rubio, J.L. Corkill, M.L. Cohen, Phys. Rev. B 49 (1994) 5081.
[34] Y. Miyamoto, A. Rubio, M.L. Cohen, S.G. Louie, Phys. Rev. B 50 (1994) 4976.
[35] Y. Miyamoto, A. Rubio, S.G. Louie, M.L. Cohen, Phys. Rev. B 50 (1994) 18360.
[36] Y. Miyamoto, M.L. Cohen, S.G. Louie, Solid State Commun. 102 (1997) 605.
[37] N. Hamada, S. Sawada, A. Oshiyama, Phys. Rev. Lett. 68 (1992) 1579.
[38] R. Saito, M. Fujita, G. Dresselhaus, M.S. Dresselhaus, Appl. Phys. Lett. 60 (1992) 2204.
[39] J.W. Mintmire, B.I. Dunlap, C.T. White, Phys Rev. Lett. 68 (1992) 631.
[40] J.W.G. Wildöer, L.C. Venema, A.G. Rinzler, R.E. Smalley, C. Dekker, Nature (London) 391 (1998) 59.
[41] T.W. Odom, J.L. Huang, P. Kim, C.M. Lieber, Nature (London) 391 (1998) 62.
[42] L. Chico, V.H. Crespi, L.X. Benedict, S.G. Louie, M.L. Cohen, Phys. Rev. Lett. 76 (1996) 971.
[43] V.H. Crespi, M.L. Cohen, A. Rubio, Phys. Rev. Lett. 79 (1997) 2093.
[44] Y. Miyamoto, A. Rubio, M.L. Cohen, S.G. Louie, Phys. Rev. Lett. 74 (1995) 2993.
[45] N.G. Chopra, R.J. Luyken, K. Cherrey, V.H. Crespi, M.L. Cohen, S.G. Louie, A. Zettl, Science 269 (1995) 966.
[46] Y. Miyamoto, S.G. Louie, M.L. Cohen, Phys. Rev. Lett. 76 (1996) 2121.
[47] P.G. Collins, A. Zettl, H. Bando, A. Thess, R.E. Smalley, Science 278 (1997) 100.
[48] P.L. McEuen, Nature 393 (1998) 15.
[49] M. Bockrath, D.H. Cobden, P.L. McEuen, N.G. Chopra, A. Zettl, A. Thess, R.E. Smalley, Science 275 (1997) 1922.
[50] S.J. Tans, M.H. Devoret, R.J.A. Groeneveld, C. Dekker, Nature 394 (1998) 761.
[51] D.H. Cobden, M. Bockrath, P.L. McEuen, A.G. Rinzler, R.E. Smalley, Phys. Rev. Lett. 81 (1998) 681.
[52] A. Zettl, N.G. Chopra, in: H. Kuzmany, J. Fink, M. Mehring, S. Roth (Eds.), Fullerenes and Fullerene Nanostructures. World Scientific, Singapore, 1996.
[53] N.G. Chopra, A. Zettl, Solid State Commun. 105 (1998) 297.
[54] P.S. Venkataramani, A.K. Mehrotra, T. Nandi, A.N. Singh, R. Bhatrager, Recent Adv. Chem. Phys. Relat. Mater., Proc. Symp. 6 (1998) Electrochemical Society.
[55] J.-M. Bonard, J.-P. Salvetat, T. Stöckli, L. Forró, A. Châtelain, Recent Adv. Chem. Phys. Relat. Mater., Proc. Symp. 6 (1998) Electrochemical Society.
[56] M.L. Cohen, S.G. Louie, A. Zettl, Solid State Commun. 113 (2000) 549.
[57] H.W. Kroto, J.R. Heath, S.C. O'Brien, R.F. Curl, R.E. Smalley, Nature 318 (1985) 162.
[58] V.H. Crespi, L.X. Benedict, M.L. Cohen, S.G. Louie, Phys. Rev. B 53 (1996) R13303.
[59] M. Côté, M.L. Cohen, D.J. Chadi, Phys. Rev. B 58 (1998) R4277.
[60] J.C. Grossman, M. Côté, S.G. Louie, M.L. Cohen, Chem. Phys. Lett. 284 (1998) 344.
[61] J.C. Grossman, S.G. Louie, M.L. Cohen, Phys. Rev. B 60 (1999) R6941.
[62] A.F. Hebard, M.J. Rosseinsky, R.C. Haddon, D.W. Murphy, S.H. Glarum, T.T.M. Palstra, A.P. Ramirez, A.R. Kortan, Nature 350 (1991) 56.
[63] J.L. Martins, Europhys. News 23 (1992) 31.
[64] L.X. Benedict, V.H. Crespi, S.G. Louie, M.L. Cohen, Phys. Rev. B 52 (1995) 14935.
[65] M. Côté, J.C. Grossman, M.L. Cohen, S.G. Louie, Phys Rev. Lett. 81 (1998) 697.